nature nanotechnology

LETTERS

PUBLISHED ONLINE: 18 OCTOBER 2009 | DOI: 10.1038/NNANO.2009.298

Self-assembled arrays of peptide nanotubes by vapour deposition

Lihi Adler-Abramovich[1†], Daniel Aronov[2†], Peter Beker[2], Maya Yevnin[2], Shiri Stempler[1], Ludmila Buzhansky[1], Gil Rosenman[2]* and Ehud Gazit[1]*

The use of bionanostructures in real-world applications will require precise control over biomolecular self-assembly and the ability to scale up production of these materials[1]. A significant challenge is to control the formation of large, homogeneous arrays of bionanostructures on macroscopic surfaces[2–4]. Previously, bionanostructure formation has been based on the spontaneous growth of heterogenic populations in bulk solution[1]. Here, we demonstrate the self-assembly of large arrays of aromatic peptide nanotubes using vapour deposition methods. This approach allows the length and density of the nanotubes to be fine-tuned by carefully controlling the supply of the building blocks from the gas phase. Furthermore, we show that the nanotube arrays can be used to develop high-surface-area electrodes for energy storage applications, highly hydrophobic self-cleaning surfaces and microfluidic chips.

Peptide building blocks provide biocompatibility, chemical versatility, biological recognition abilities and facile synthesis, which make them an attractive organic building block for bionanotechnology applications[5–10]. The recently identified aromatic dipeptide nanotubes (ADNTs) are a family of well-ordered nanostructures that can be self-assembled from simple building blocks[11]. These nanostructures have notable chemical and physical properties, including thermal and chemical stability[12,13] and significant rigidity at the nanoscale[14,15]. The nanometric dimensions of ADNTs have already been used in the fabrication of a sensitive biosensing device[16] and as a casting mould for the fabrication of metallic nanowires[11,17]. The ability to form 'nanoforests' composed of vertically aligned nanotubes and to horizontally align modified and non-modified tubes in a magnetic field has also been demonstrated previously[18,19]. ADNTs can be patterned using inkjet technology[20] and arranged on surfaces with controllable wettability using low-energy electron irradiation[21].

Coating a substrate with ADNTs results in a considerable increase in substrate surface area[16], which is important in the development of applications such as effective electrochemical units and superhydrophobic coatings for microfluidic devices, smart windows and solar cells. This, combined with their bio-inspired nature, makes ADNTs attractive for bionanotechnology applications.

Because ADNTs are formed from low-molecular-weight (312 Da) building blocks, and because of the inherent volatility of aromatic systems, these structures appeared to be excellent candidates for use in industrial vapour deposition methods, as used previously for inorganic and carbon nanostructures[2–4,22]. Here, we report the use of such vapour deposition methods in the fabrication of highly oriented and aligned ADNTs. This method allows the biological elements to be densely and homogeneously coated over large areas. The thickness of the coating is controllable, and patterned arrays can be fabricated.

The diphenylalanine peptide lyophilized powder was placed in a vacuum chamber and evaporated at a temperature of 220 °C (Fig. 1). Figure 2 shows typical top and side view scanning electron microscopy (SEM) images of the deposited ADNTs. The SEM data show a normally oriented, homogeneously distributed array of nanotubes with a density of 4×10^8 nanotubes cm^{-2}. It should be noted that the evaporation system allows the deposition of ADNT arrays as a uniform layer on large surface areas of up to 10 cm^2. The nanotubes are several micrometres in length, with diameters ranging from 50 to 300 nm (Fig. 2b). The morphology of these nanotubes is similar to the morphology of ADNTs that self-assemble in solution[11,23]. The majority of the structures are hollow tubes; however, in the self-assembly process, the ends of some of the tubes can become narrow (Supplementary Fig. S1).

The average length, thickness and surface density of these nanotubes can be controlled by adjusting the deposition parameters. Figure 2c shows a side view of a thick array of nanotubes of length 40 μm, whereas Fig. 2d shows a side view of a thin array of nanotubes of length 5 μm. Thickness control was achieved by altering the deposition time, using times of 2 min (Fig. 2d) and 10 min (Fig. 2c), respectively.

The chemical structure of the self-assembled nanotubes was examined using time-of-flight secondary ion spectroscopy (ToF-SIMS; Supplementary Fig. S2) and high-performance liquid chromatography (HPLC). The ToF-SIMS positive ion spectrum shows a characteristic peak at 295 m/z (mass to charge ratio), which corresponds to the MH^+ in Cyclo–Phe–Phe (Supplementary Fig. S2). Together with HPLC analysis, the results indicate backbone cyclization of the diphenylalanine peptide during the vapour deposition procedure, which results in the formation of nanotubes composed of diketopiperazine, Cyclo–Phe–Phe dipeptide (see Supplementary Information). Previous studies of self-assembled Cyclo–Phe–Phe peptide in solution revealed the formation of similar tubular structures[23]. It is suggested that the linear peptide H–Phe–Phe–OH is subject to cyclization during the vapour deposition process. The stacking of aromatic residues has a key role in the process of molecular recognition and self-assembly that leads to the formation of these ordered structures and stabilizes the formed structures[11,23,24]. The restricted geometry and the attractive forces of the aromatic moieties provide order and directionality as well as the energetic contribution needed for the formation of such well-ordered structures[23] (Fig. 1).

Furthermore, proteolytically stable building blocks based on the D-amino acid analogue of the peptide (H–(D)Phe–(D)Phe–OH) were used to form vertically aligned ADNTs using the same vapour

[1]Department of Molecular Microbiology and Biotechnology, George S. Wise Faculty of Life Sciences, Tel Aviv University, 69978 Tel Aviv, Israel, [2]Department of Physical Electronics, School of Electrical Engineering, Tel Aviv University, 69978 Tel Aviv, Israel; †These authors contributed equally to this work.
*e-mail: gilr@eng.tau.ac.il; ehudg@post.tau.ac.il

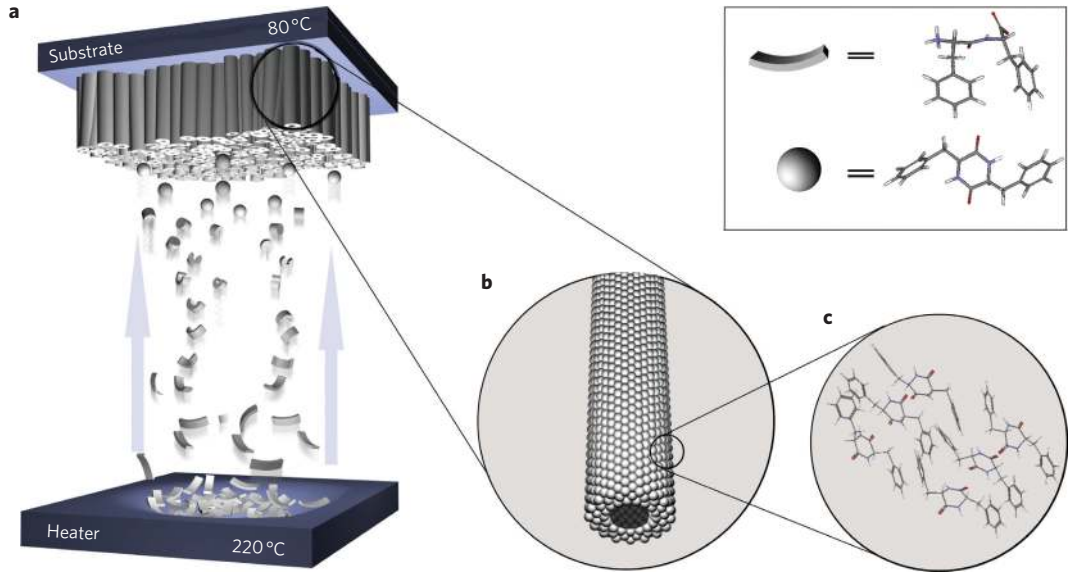

Figure 1 | Proposed assembly mechanism for the formation of vertically aligned ADNTs. a, Schematic of the vapour deposition technique. During evaporation, the diphenylalanine peptide, which is heated to 220 °C, attained a cyclic structure (Cyclo-Phe-Phe peptide) and then assembled on a substrate to form ordered vertically aligned nanotubes. **b**, Illustration of a single peptide nanotube composed mainly of Cyclo-Phe-Phe peptide. **c**, Molecular arrangement of six Cyclo-Phe-Phe peptides after energy minimization. A stacking interaction between aromatic moieties of the peptides is suggested to provide the energetic contribution as well as order and directionality for the initial interaction.

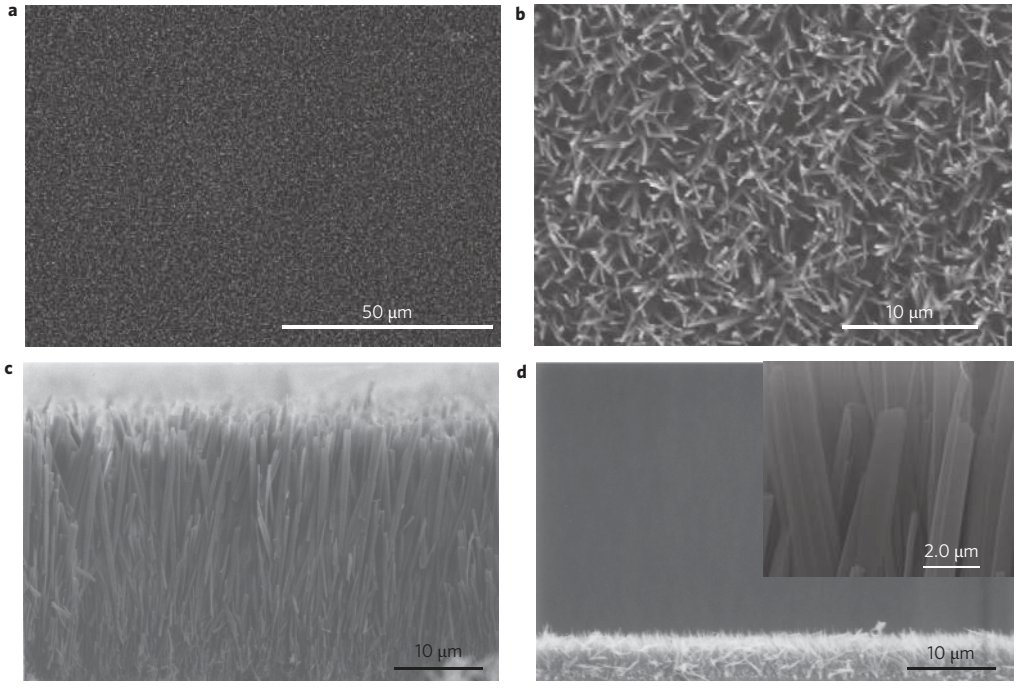

Figure 2 | Vapour deposition of vertically aligned ADNTs. a, Top-view SEM image of the ADNTs after the vapour deposition process. **b**, High-resolution top-view SEM image of the ADNTs after vapour deposition. **c**, Side view of vertically aligned ADNTs demonstrating the elongated micrometre tubes, with a thickness of 40 μm. **d**, Side view of vertically aligned ADNTs demonstrating the elongated micrometre tubes, with a thickness of 5 μm. The inset shows a high-resolution SEM image of the ADNTs.

deposition technique. This peptide formed nanotubes with the same structural features as the corresponding L-amino acid peptide (Supplementary Fig. S3). To investigate the structural characteristics of our samples, we carried out X-ray diffraction (XRD) analysis. The XRD patterns of the deposited ADNT layers exhibit a number of diffraction peaks, indicating the highly crystalline nature of the ADNT arrays (Supplementary Fig. S4a). The XRD pattern of the vapour-deposited ADNTs differs from that of ADNTs self-assembled in solution[18]. We attribute the difference in XRD patterns to the change in the peptide, in particular the cyclization of the backbone that occurs during the vapour deposition process. Grazing incidence wide-angle X-ray diffraction (WAXD) measurements were also made, with the beam perpendicular to the long axis of the nanostructures and parallel to the substrate. The

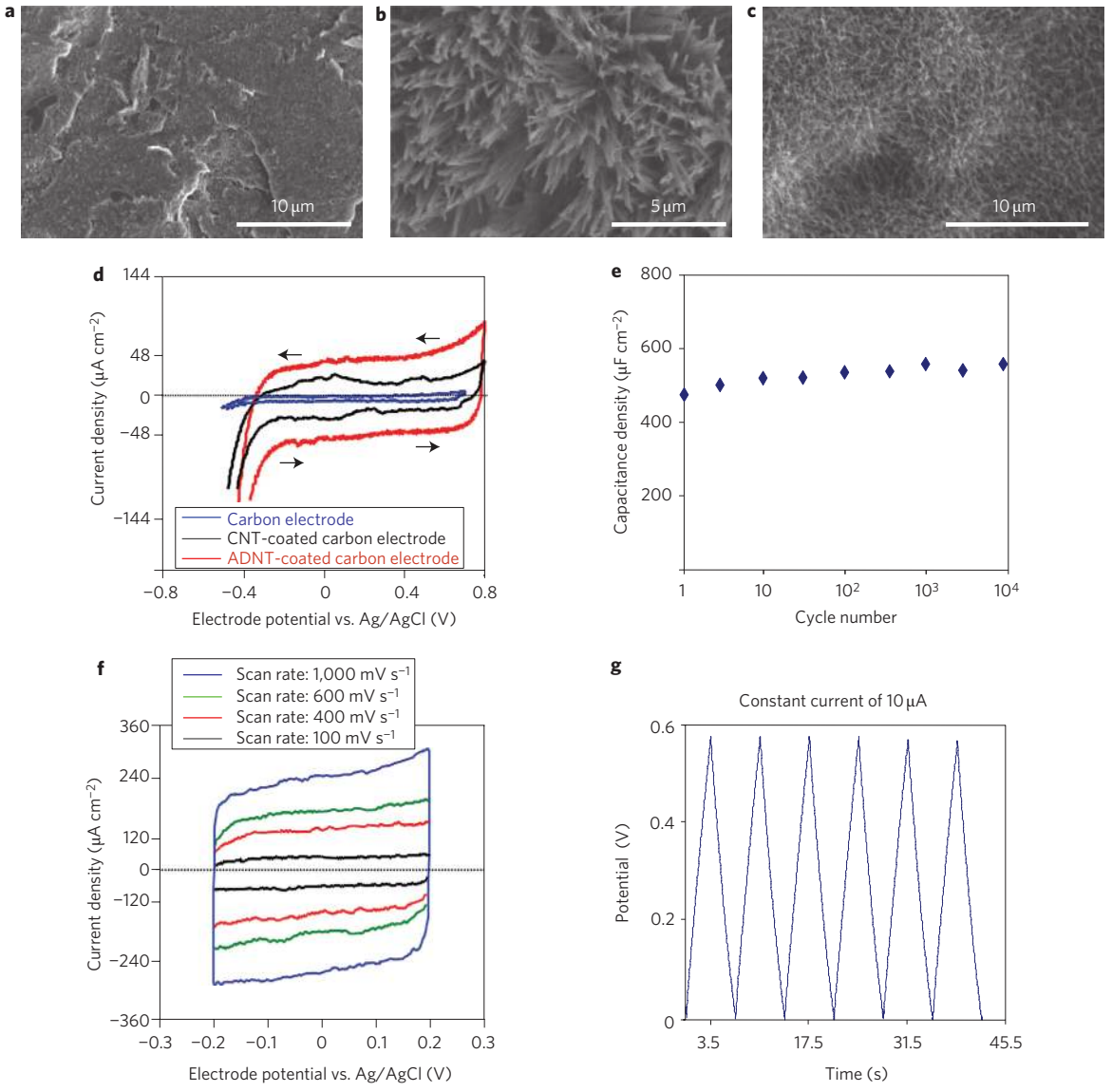

Figure 3 | Ultracapacitors based on ADNT-coated electrodes. a–c, Top-view SEM images of uncoated (**a**), ADNT-coated (**b**) and carbon-nanotube-coated (**c**) electrodes. **d**, Cyclic voltammetry measurements of ADNT-coated (red line), carbon-nanotube-coated (black line) and uncoated (blue line) carbon electrodes. **e**, Cyclability tests of the ADNT-coated carbon electrodes, cycled 10,000 times. **f**, Cyclic voltammograms at different scan rates of an ADNT-coated carbon electrode. **g**, Charge/discharge curve of an ADNT-coated carbon electrode at constant current (10 μA).

appearance of diffraction arcs provides evidence for the preferred orientation of some of the constituent crystallites in the nanotube array (Supplementary Fig. S4a,b).

Ultracapacitors are promising energy storage devices due to their unique combination of high power density and relatively large energy density. They are based on electrostatic energy storage of a charged double layer (Helmholtz layer) formed by the separated electronic and ionic charges at the interface of the electrode material and electrolyte solution. Porous electrodes and nanostructural coatings such as carbon nanotubes and carbon fibres have been used previously[25].

We developed electrostatic ultracapacitors based on ADNT-modified carbon electrodes. The formation of an ADNT array extends the functional surface area of the ultracapacitor electrode and significantly increases its capacitance. ADNT nanoforest modified ultracapacitor electrodes were compared with standard carbon electrodes and carbon-nanotube-coated carbon electrodes (Fig. 3a–c). Figure 3d depicts cyclic voltammetry characteristics for these three electrodes. The characteristic anodic and cathodic electrochemical redox Faradaic processes begin at the applied potentials −0.2 V and +0.6 V, regardless of the origin of the electrode coating. The remaining area of the cyclic voltammograms inside the tested potential range shows a rectangular current response that is symmetrical around the zero-current line for all the electrodes.

The current response for the ADNT-modified electrode was found to be 30 times higher than that for an unmodified carbon electrode (Fig. 3d). Estimation suggests that ADNT modification of carbon electrodes (Fig. 3d) leads to significant growth of the electrical double-layer capacitance density, reaching $C_{DL} = 480\ \mu F\ cm^{-2}$ for a geometric electrode area; in contrast, $C_{DL} = 16\ \mu F\ cm^{-2}$ for the carbon electrode. The same phenomenon was observed when comparing ADNT-modified carbon electrodes with carbon-nanotube-modified electrodes, which had a double-layer capacitance density of $C_{DL} = 120\ \mu F\ cm^{-2}$. The determined capacitance density of the ADNT-modified carbon electrode was found to have high values when compared with the C_{DL} values published in the literature for the same potential scan rate[26,27].

Ideal double-layer capacitance behaviour of an electrode material is expressed in the form of a rectangular shape of voltammetry characteristics as observed in Fig. 3d. These data show that the sign of the current is immediately reversed upon reversal of the potential sweep. Thus the observed charge/discharge process of the ADNT-modified electrodes is purely electrostatic and the current is independent of the applied potential. The observed pronounced difference in the current density response and double-layer capacitance for carbon-nanotube-modified and ADNT-modified electrodes compared with carbon electrodes (Fig. 3d) may be ascribed to the electrode modification and the increase in functional area of the ADNT-modified electrodes. However, the data also show that the ADNT-based electrode has a much higher double-layer capacitance compared with that of carbon-nanotube-modified electrodes.

The cyclic voltammogram studies and SEM images did not reveal any variation of ADNT-modified electrodes after two weeks of immersion in the aqueous electrolyte. Our studies revealed no significant difference in double-layer capacitance C_{DL} values, even after continuous measurements over 10,000 charge/discharge cycles (Fig. 3e). This fact was verified by SEM imaging. These observations serve as direct evidence for the high chemical stability and good adhesion property of the ADNT electrode coatings in the tested electrolyte. Figure 3f presents the cyclic voltammograms with different scan rates of the ADNT-modified electrode. The profile of the cyclic voltammogram curves at a scan rate of 100 mV s^{-1} is almost ideally rectangular and retains such a shape even at the very high scan rate of 1,000 mV s^{-1}, therefore showing ideal capacitive behaviour.

A typical constant current charge/discharge curve of the ADNT-modified electrodes is shown in Fig. 3g. As can be seen, the potential–time (V–t) responses of the charge process are almost a mirror image of their corresponding discharge counterparts. No potential drop was observed, reflecting the small equivalent series resistance of the electrodes.

The formation of ordered nanoarrays could be used not only for enhancing the functional surface area as with ultracapacitors, but also to modify the physical properties of various surfaces for other applications. Thus, another application for ADNT arrays is the formation of highly hydrophobic surfaces. Preparation of highly hydrophobic surfaces is based on a combination of surface micro-nanotexturing (lotus-type structure) and the use of a surface comprising a low surface energy material[28]. The highly hydrophobic coats may be used for self-cleaning surfaces, smart windows and solar cells. They are also the key elements for the tailoring of built-in structures for microfluidic devices.

An ADNT nanostructural coating was tailored using the vapour deposition technique, by the self-organization of vertically aligned ADNTs (Fig. 1). A large-scale coated area consists of individual nanotubes with a high aspect ratio (reaching 1:100). It represents a 'lotus-type' array of ADNT nano-units, which have very high hydrophobic properties at a macroscopic scale. Such a built-in bio-nanotexture leads to observation of new surface phenomenon—ADNT-based high hydrophobicity.

The fabrication of ADNT coatings was performed using the vapour deposition technique on glass substrates. We obtained a significant eightfold (approx.) increase in hydrophobicity using normally orientated ADNTs when compared with bare glass. The measured water droplet contact angle on the modified surface was $\theta \approx 125^\circ$ (Fig. 4a,b), which compares with a contact angle of $\theta \approx 15^\circ$ for the unmodified glass surface. Fine control of the peptide-modified surface hydrophobicity may be achieved by varying the number of phenylalanine residues in the peptide building block. We modified the glass surfaces using vapour deposition with tri-, tetra- and pentaphenylalanine peptides (Supplementary Fig. S5). Figure 4c shows monotonic growth of the water contact angle θ as a function of the peptide's length (the number of phenylalanine residues), due to the physicochemical structure of the phenylalanine. A high hydrophobicity, with a contact angle of $\theta \approx 140^\circ$, was obtained on pentaphenylalanine-modified surfaces, resulting in the fabrication of highly hydrophobic coatings.

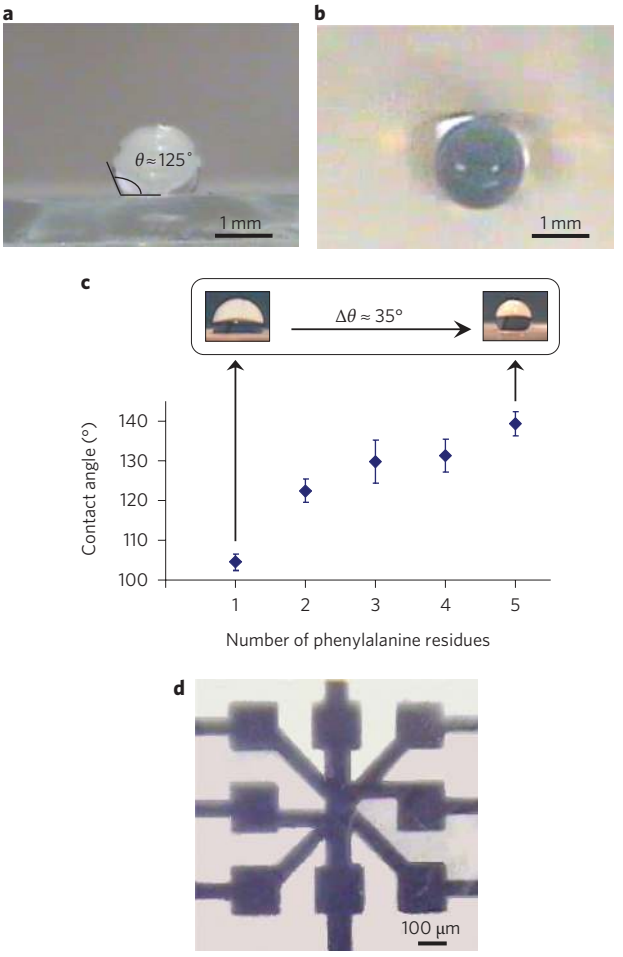

Figure 4 | Highly hydrophobic surfaces and microfluidic patterning. **a**,**b**, Side view (**a**) and top view (**b**) of the apparent contact angle of the deionized water on the ADNT-coated glass surface. The contact angle is $\theta \approx 125^\circ$. **c**, Water contact angle θ as a function of the length of the peptide building blocks (Phe). **d**, ADNT-coated patterning on a silicon dioxide surface. The bright regions are highly hydrophobic (non-wettable) ADNT-coated areas, and the dark regions correspond to uncoated silicon dioxide areas covered by water.

This technique also allows the construction of an ADNT-based microfluidic chip. We recently demonstrated the usefulness of ADNTs in nanofluidics applications, but we could not control the formation of large-scale arrays[29]. Here, a silicon dioxide substrate was patterned with ADNTs using vapour deposition of diphenylalanine peptide through a shadow mask of the designed structure. Figure 4d presents the silicon dioxide surface with patterned channels and patches that may be used in a microfluidic system. High wettability water contrast is provided by the non-wettable (hydrophobic) regions covered by ADNTs, whereas the original silicon dioxide surface is hydrophilic, with a contact angle of $\theta \approx 10^\circ$. The patterned surface was exposed to water vapour at a relative humidity of 50% and then cooled to 5 °C below the dew point. Consequently, the water condensed on the hydrophilic regions, producing liquid micro-channels. In this way, it is possible to create microfluidic structures for different purposes with a large variety of morphologies. Thus, by using the array of ADNT

hydrophobic patterns, it is possible to control the capillary flow speed and obtain a proper delay stage at a specific position within the microchannels.

In summary, we have demonstrated the formation of self-assembled arrays of biomolecular structures using vapour deposition. This industry-standard deposition method could enable the fabrication of ADNT-based devices and surfaces with the facility to be scaled up. The potential applications for this material are wide ranging and include energy storage, smart windows and microfluidic devices. Furthermore, the previous industrial application of aspartyl-phenylalanine methyl ester (the aspartame sweetener) suggests that the large-scale production of a dipeptide could be more cost-effective than that of inorganic and carbon nanostructures.

Methods

Vertical alignment of diphenylamine peptide nanotubes using thermal evaporation. ADNTs were deposited on different substrates, such as carbon, glass, gold and silicon dioxide using a biomolecule vapour deposition method (Fig. 1). In a typical synthesis, ~1 mg of diphenylalanine peptide lyophilized powder (Bachem) was placed in a small copper boat to serve as the source material. The substrate was placed above the source at a vertical distance of ~2 cm. The chamber was then set to 220 °C with a heating rate of 10 °C min^{-1} at a constant pressure of 1×10^{-5} mbar. Control of ADNT thickness was achieved by varying the deposition time (Δt = 2–10 min). The resulting products were collected on the downward-facing side of the substrate. Some of the samples deposited on the substrate were heated to 200 °C.

Scanning electron microscopy. Samples were coated with palladium–gold and analysed using a JSM JEOL 6300 scanning electron microscope operating at 5 kV. Images were taken to obtain a top view or rotated at 90° to allow the side view to be imaged.

Determination of surface area. The morphology of the ADNT surfaces was characterized by SEM analysis. An image-processing algorithm, using MATLAB® software, was implemented to obtain quantitative information concerning the macroscopic characteristics of the ADNT coating. This method is routinely used to determine the distribution of particle size and seemed simple and appropriate in this case. The information was derived from 50 top and side-view SEM images of 20 different ADNT samples.

High-performance liquid chromatography. The ADNTs were deposited on the glass surface using the vapour deposition technique, then peeled off. The references peptide H–(L)Phe–(L)Phe–OH and Cyclo–Phe–Phe were purchased from Bachem and H–(L)Phe–(D)Phe–OH and H–(D)Phe–(L)Phe–OH from Peptide 2.0. All the peptides were dissolved in 1,1,1,3,3,3-hexafluoro-2-propanol (HFIP) at a concentration of 20 mM, then diluted in acetonitrile to a final concentration of 10 mM. HPLC was carried out using a C-18 column at an isocratic condition of 50% acetonitrile in H_2O.

Time-of-flight secondary ion spectroscopy. ToF-SIMS analysis was carried out to characterize the chemical structure and elemental composition contained on the ADNT-coated surfaces using a Physical Electronics TRIFT II ToF-SIMS instrument using a 15-kV Ga^+ primary ion gun.

X-ray diffraction and grazing incidence wide-angle X-ray diffraction (WAXD) measurements. The ADNT array was formed on siliconized glass. The ADNT array deposited from the vapour phase was subjected to XRD analysis. XRD measurements were made using a TTrax III theta–theta diffractometer (Rigaku) with copper anode, parallel beam optics and generator power of 12 kW. WAXD measurements were obtained using a Searle camera fixed to an Elliott GX6 generator with copper anode, operating at 1.2 kW. The X-ray beam was perpendicular to the long axis of the nanostructures and parallel to the siliconized glass surface, which was held in the horizontal plane. Two-dimensional detection was achieved using Fuji imaging plates, which were scanned and digitized using a home-made reader.

Cyclo–Phe–Phe peptide energy minimization study. The initial Cyclo–Phe–Phe peptide conformation was optimized using an MM2 force field. An energy minimization study for six molecules was performed using the CHARMm force field with Smart Minimizer algorithm (Discovery Studio 2.0). The energy was calculated as follows: potential energy = −210.02781 kcal mol^{-1}; van der Waals energy = −50.72428 kcal mol^{-1}; electrostatic energy = −226.82887 kcal mol^{-1}. This represents the lowest energy for the molecular organization out of 15 initial conformations that were computationally studied.

Electrochemical measurements. Electrochemical tests for three types of electrodes (carbon, carbon-nanotube-coated and ADNT-modified carbon) were performed using a potentiostat/galvanostat (EG&G Princeton Applied Research, Model 273A). The results for the ADNT-coated carbon electrodes were compared with those of commercially available carbon-nanotube-modified and carbon electrodes (DropSens). All working electrodes had an identical geometric area of 0.125 cm^2. The electrochemical units comprised the basic working electrode made of carbon, a counter electrode of carbon, and a silver/silver chloride electrode that was used as a reference electrode. The electrolyte was a standard inorganic solution 0.05 M KH_2PO_4 and 0.5 M KCl. A potential difference was applied to the cells and the reduction/oxidation current density measured at room temperature over a potential window from −0.5 to +0.8 V (versus Ag/AgCl) and then from +0.8 to −0.5 V at a potential scan rate of 100 mV s^{-1}. The double-layer capacitance C_{DL} was measured directly from the recorded cyclic voltammetry graphs over potential ranges essentially free of faradaic processes. The capacitance was directly estimated from the experimental graph using the simple expression

$$\frac{I}{(\partial V/\partial t)} = C_{DL} \text{ (in farads)}$$

where C_{DL} is the double-layer capacitance, I is the recorded electric current of the charge/discharge process, and $\partial V/\partial t$ is the potential sweep rate[28]. The C_{DL} values for the three studied electrodes (carbon, carbon-nanotube-coated and ADNT-coated) were estimated by normalizing the experimentally measured C_{DL} to the electrode geometric surface area.

Microfluidic patterning preparation. The silicon dioxide substrate was patterned with ADNTs using vapour deposition of diphenylalanine peptide through a shadow mask of the designed structure. High wettability water contrast was provided by non-wettable (hydrophobic) regions covered by ADNTs and the original silicon dioxide surface (hydrophilic with $\theta \approx 10°$). The patterned surface was exposed to water vapour at a relative humidity of 50% and then cooled to a temperature of 5 °C below the dew point. The water condensed on the hydrophilic regions and produced liquid micro-channels. In this manner, it is possible to create microfluidic structures for different purposes with a large variety of morphologies.

Preparation and measurement of highly hydrophobic surfaces. The wettability states of ADNT-coated substrates were estimated by measuring the static contact angle of sessile drops of deionized water (pH, 5.5; resistivity, >17 MΩ cm) placed on a sample surface. Optical inspections of the wettability properties were performed using a specially designed system combining two charge-coupled device cameras that allowed side and top view inspection. The volume of liquid was kept constant (2 μl) for all contact angle measurements of different specimens. Contact angles were calculated using computer software that fit a solution of the Young–Laplace equation to the measured radius of the base of the drop, given its volume, surface energy and density. The wettability investigations were carried out with an accuracy of ±1° at a temperature of 26±1 °C and a relative humidity of 45±5%.

Received 26 May 2009; accepted 7 September 2009; published online 18 October 2009

References

1. Zhang, S. Fabrication of novel biomaterials through molecular self-assembly. *Nature Biotechnol.* **21,** 1171–1178 (2003).
2. Modi, A., Koratkar, N., Lass, E., Wei, B. Q. & Ajayan, P. M. Miniaturized gas ionization sensors using carbon nanotubes. *Nature* **424,** 171–174 (2003).
3. Thurn-Albrecht, T. *et al.* Ultrahigh-density nanowire arrays grown in self-assembled diblock copolymer templates. *Science* **290,** 2126–2129 (2000).
4. Zhong, Z. H., Wang, D. L., Cui, Y., Bockrath, M. W. & Lieber, C. M. Nanowire crossbar arrays as address decoders for integrated nanosystems. *Science* **302,** 1377–1379 (2003).
5. Aggeli, A. *et al.* Responsive gels formed by the spontaneous self-assembly of peptides into polymeric beta-sheet tapes. *Nature* **386,** 259–262 (1997).
6. Banerjee, I. A., Yu, L. & Matsui, H. Cu nanocrystal growth on peptide nanotubes by biomineralization: size control of Cu nanocrystals by tuning peptide conformation. *Proc. Natl Acad. Sci. USA* **100,** 14678–14682 (2003).
7. Ghadiri, M. R., Granja, J. R., Milligan, R. A., McRee, D. E. & Hazanovich, N. Self-assembling organic nanotubes based on a cyclic peptide architecture. *Nature* **366,** 324–327 (1993).
8. Hartgerink, J. D., Beniash, E. & Stupp, S. I. Self-assembly and mineralization of peptideamphiphile nanofibers. *Science* **294,** 1684–1688 (2001).
9. Mao, C. *et al.* Viral assembly of oriented quantum dot nanowires. *Science* **303,** 213–217 (2004).
10. Vauthey, S., Santoso, S., Gong, H., Watson, N. & Zhang, S. Molecular self-assembly of surfactant-like peptides to form nanotubes and nanovesicles. *Proc. Natl Acad. Sci. USA* **16,** 5355–5360 (2002).
11. Reches, M. & Gazit, E. Casting metal nanowires within discrete self-assembled peptide nanotubes. *Science* **300,** 625–627 (2003).
12. Sedman, V. L., Adler-Abramovich, L., Allen, S., Gazit, E. & Tendler, S. J. Direct observation of the release of phenylalanine from diphenylalanine nanotubes. *J. Am. Chem. Soc.* **128,** 6903–6908 (2006).
13. Adler-Abramovich, L. *et al.* Thermal and chemical stability of diphenylalanine peptide nanotubes: implications for nanotechnological applications. *Langmuir* **22,** 1313–1320 (2006).

14. Kol, N. *et al.* Self-assembled peptide nanotubes are uniquely rigid bioinspired supramolecular structures. *Nano Lett.* **5,** 1343–1346 (2005).
15. Niu, L., Chen, X., Allen, S. & Tendler, S. J. B. Using the bending beam model to estimate the elasticity of diphenylalanine nanotubes. *Langmuir* **23,** 7443–7446 (2007).
16. Yemini, M., Reches, M., Rishpon, J. & Gazit, E. Novel electrochemical biosensing platform using self-assembled peptide nanotubes. *Nano Lett.* **5,** 183–186 (2005).
17. Song, Y. *et al.* Synthesis of peptide–nanotube platinum–nanoparticle composites. *Chem. Commun.* **9,** 1044–1045 (2004).
18. Reches, M. & Gazit, E. Controlled patterning of aligned self-assembled peptide nanotubes. *Nature Nanotech.* **1,** 195–200 (2006).
19. Hill, R. J. A. *et al.* Alignment of aromatic peptide tubes in strong magnetic fields. *Adv. Mater.* **19,** 4474–4479 (2007).
20. Adler-Abramovich, L. & Gazit, E. Controlled patterning of peptide nanotubes and nanospheres using inkjet printing technology. *J. Pept. Sci.* **14,** 217–223 (2008).
21. Adler-Abramovich, L., Aronov, D., Gazit, E. & Rosenman, G. Patterned arrays of ordered peptide nanostructures. *J. Nanosci. Nanotech.* **9,** 1701–1708 (2008).
22. Fan, S. *et al.* Self-oriented regular arrays of carbon nanotubes and their field emission properties. *Science* **283,** 512–514 (1999).
23. Reches, M. & Gazit, E. Self-assembly of peptide nanotubes and amyloid-like structures by charged-termini capped diphenylalanine peptide analogues. *Isr. J. Chem.* **45,** 363–371 (2005).
24. Gorbitz, C. H. The structure of nanotubes formed by diphenylalanine, the core recognition motif of Alzheimer's β-amyloid polypeptide. *Chem. Commun.* 2332–2334 (2006).
25. An, K. H. *et al.* Supercapacitors using single-walled carbon nanotube electrodes. *Adv. Mater.* **13,** 497–500 (2001).
26. Kötz, R. & Carlen, M. Principles and applications of electrochemical capacitors. *Electrochim. Acta* **45,** 2483–2498 (2000).
27. Baughman, R. H., Zakhidov, A. A. & de Heer, W. A. Carbon nanotubes—the route toward applications. *Science* **297,** 787–792 (2002).
28. Genzer, J. & Efimenko, K. Recent developments in superhydrophobic surfaces and their relevance to marine fouling: a review. *Biofouling* **22,** 339–360 (2006).
29. Sopher, N. B., Abrams, Z. R., Reches, M., Gazit, E. & Hanein, Y. Integrating peptide nanotubes in micro-fabrication processes. *J. Micromech. Microeng.* **17,** 2360–2365 (2007).

Acknowledgements

The authors would like to thank E. Wachtel for help with the XRD analysis, D. Shabat and R. Perry for help with HPLC analysis, N. Fishelson for helpful discussions regarding the electrochemistry results, E. Strauss for help with ToF-SIMS analysis, R. Persky and I. Ulanovsky for help with liquid chromatography-mass spectrometry (LC-MS) analysis, Z. Barkay for help with the SEM analysis, T. Mazor for graphical assistance, and L. Leiserowitz, Y. Feldman and members of the Gazit laboratory for helpful discussions. E.G. acknowledges the support of the DIP German-Israel Cooperation Program. L.A.A. gratefully acknowledges the support of the Colton Foundation.

Author contributions

L.A.A, D.A., E.G. and G.R. conceived and designed the experiments. L.A.A., D.A., P.B. and M.Y. planned and performed the experiments. L.A.A., D.A., E.G., G.R. and L.B. analysed the data. S.S. performed the energy minimization study. L.A.A., D.A., E.G. and G.R. co-wrote the paper. All authors discussed the results and commented on the manuscript.

Additional information

Supplementary information accompanies this paper at www.nature.com/naturenanotechnology. Reprints and permission information is available online at http://npg.nature.com/reprintsandpermissions/. Correspondence and requests for materials should be addressed to G.R. and E.G.